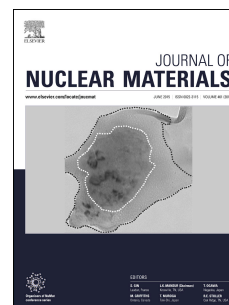


Accepted Manuscript

In-situ TEM study of radiation-induced amorphization and recrystallization of hydroxyapatite

Jianren Zhou, Tiankai Yao, Dongmei Cao, Jie Lian, Fengyuan Lu



PII: S0022-3115(18)30547-6

DOI: [10.1016/j.jnucmat.2018.10.018](https://doi.org/10.1016/j.jnucmat.2018.10.018)

Reference: NUMA 51257

To appear in: *Journal of Nuclear Materials*

Received Date: 16 April 2018

Revised Date: 10 October 2018

Accepted Date: 10 October 2018

Please cite this article as: J. Zhou, T. Yao, D. Cao, J. Lian, F. Lu, In-situ TEM study of radiation-induced amorphization and recrystallization of hydroxyapatite, *Journal of Nuclear Materials* (2018), doi: <https://doi.org/10.1016/j.jnucmat.2018.10.018>.

This is a PDF file of an unedited manuscript that has been accepted for publication. As a service to our customers we are providing this early version of the manuscript. The manuscript will undergo copyediting, typesetting, and review of the resulting proof before it is published in its final form. Please note that during the production process errors may be discovered which could affect the content, and all legal disclaimers that apply to the journal pertain.

Manuscript to be submitted to the Journal of Nuclear Materials

In-situ TEM Study of Radiation-induced Amorphization and Recrystallization of Hydroxyapatite

Jianren Zhou,[‡] Tiankai Yao,[§] Dongmei Cao,[‡] Jie Lian,[§] Fengyuan Lu^{‡,†}

[‡]Department of Mechanical and Industrial Engineering, Louisiana State University, Baton Rouge, LA 70803, USA

[§]Department of Mechanical, Aerospace, and Nuclear Engineering, Rensselaer Polytechnic Institute, Troy, NY 12180, USA

[†]Corresponding author. Email: luf@lsu.edu; Tel: 225-578-7953.

Abstract

The radiation response of hydroxyapatite, a nuclear waste form candidate, was investigated using 1 MeV Kr²⁺ and 200 keV electron irradiations combined with *in-situ* TEM observation. The results showed a remarkable difference in the behavior of nano-crystalline hydroxyapatite under the two different radiation conditions. A crystalline-to-amorphous transformation occurred under the 1 MeV Kr²⁺ irradiation due to the accumulation of displacement damage, with a critical amorphization dose (D_c) of 2×10^{14} ions/cm² (0.05 dpa) at room temperature. The D_c increased dramatically with temperature due to effective dynamic annealing of radiation-induced defects, such that no amorphization occurred above a critical temperature (T_c) of 545 K. In contrast, under 200 keV electron irradiation, which mainly dissipates its energy through inelastic ionization processes, the pre-amorphized hydroxyapatite exhibited rapid recrystallization, likely due to the bond breaking and reforming at the amorphous-crystalline interface assisted by the ionization. The electron-irradiation induced recrystallization in amorphous hydroxyapatite was extremely sensitive, with a critical electron dose several orders of magnitude lower than most previously reported ceramics. Under concurrent ion and electron irradiations, the materials retained crystalline even at the critical dose of 0.05 dpa, and remained so until the dose reached 0.15 dpa, lending further proof to the enhanced defect recovery by ionizing electrons. The radiation data of hydroxyapatite highlights the material's sensitivity to radiation conditions and its excellent dynamic defect annealing ability.

Keywords: Radiation effects; Nano-crystalline hydroxyapatite; Amorphization; Recrystallization

1. Introduction

Apatite is an earth abundant mineral with a chemical formula of $A_{10}(BO_4)_6X_2$ ($A = Ca, Pb$, rare earth, fission product elements, or actinides; $B = P, V, Si$ or Cr ; $X = OH, O$ or halogens). Due to its extraordinary crystal chemistry, structure flexibility, promising thermal stability and low leaching rate, the apatite structure-type has been proposed as a potential crystalline ceramic waste form for high level nuclear waste, particularly for actinide and fission product bearing waste streams. However, ceramic-based nuclear waste forms can undergo atomic scale changes (radiation damage and transmutation) caused by β -decay of the fission products and α -decay of the actinide elements, which can significantly affect their performance. Energetic ion irradiation-induced amorphization of crystalline ceramic waste form materials has been reported in monazite[1], pyrochlore[2], apatite[3] and britholite[4]; on the other hand, under electron irradiation in the sub-MeV energy range, a few ceramic materials exhibit a remarkable defect recovery behavior[1, 5-8], prompting further efforts to fully understand the radiation stability of ceramics for nuclear waste management applications.

The present study focuses on the radiation stability of hydroxyapatite (HAp), an important nuclear waste form candidate. HAp, with a stoichiometric composition of $Ca_{10}(PO_4)_6(OH)_2$, is the main constituent of animal bones and has a poorly crystalline non-stoichiometric nano-sized structure[9]. Pure HAp has thermal stability identified by its resistance to undergo any phase transformation up to $1300^\circ C$ [10]. Due to its high chemical durability, unique structure and low cost, HAp has been proposed as a candidate for the removal and storage of a range of radionuclides, both alpha and beta emitters, including strontium[11, 12], uranium, plutonium, neptunium[13, 14], and iodine isotopes[15, 16]. The HAp derived from animal bones is nano-crystalline, which is expected to have improved exchange and uptake capacities when compared to their micron-sized analogues due to their increased surface area, significant fraction of defective sites. But the effect of nanostructure on the radiation stability in this case is still unclear, even though the high density of grain boundaries/interfaces is believed by many to have the capability of mitigating defect accumulation [17-20]. The current research on HAp in the context of nuclear waste management mostly address the questions of radionuclide removal, immobilization, waste form fabrication and leaching properties. However, little experimental work has been done to understand the radiation stability of the nano-crystalline HAp, which is crucial to be considered in the design of nuclear waste form. To fill the gap in the radiation

behavior of HAp we conducted irradiations of the nano-crystalline HAp, derived from bovine bones, using displacive ion-beam irradiation (1 MeV Kr^{2+}) and ionizing electron-beam irradiation (200 keV electrons), respectively, to reveal its response to various radiation conditions.

2. Experimental Procedures

Nano-crystalline HAp was prepared by calcining a small amount of bovine bone in muffle furnace (Thermo scientific model number F48020-80). The calcination temperature was increased from room temperature at a rate of $8^\circ\text{C}/\text{min}$ until the target temperature of 600°C was reached and then maintained for 60 minutes. The sample was then furnace cooled to room temperature and ground into fine powder by mortar and pestle. The as-prepared powder was referred to as HAp-600C throughout the text. By utilizing an X'Pert Pro X-ray diffractometer, the crystal structure of the as-calcined sample was determined and confirmed as $\text{Ca}_{10}(\text{PO}_4)_6(\text{OH})_2$ of the apatite-type structure using X-ray diffraction (XRD); this structure was further confirmed through Rietveld refinement of the XRD data of the sample, as shown in Fig. 1.

Displacive ion irradiation of the HAp-600C was conducted with 1 MeV Kr^{2+} , and the microstructural changes were monitored with *in situ* transmission electron microscopy (TEM) using the IVEM Tandem Facility at the Argonne National Laboratory (ANL). The IVEM-Tandem Facility consists of a Hitachi H-9000NAR TEM with an NEC Tandem ion accelerator, which enables *in situ* TEM observation of material behaviors under intensive ion bombardments. To understand the effect of temperature on the irradiation damage process, the HAp-600C samples were irradiated at different temperatures ranging from 298 K to 523 K by use of a heating stage equipped to the TEM. The apatite structure has been known to undergo a crystalline-to-amorphous transformation under intensive displacive ion irradiations. The amorphization process was closely monitored by *in situ* selected area electron diffraction (SAED) patterns, as well as dark field TEM imaging by inserting an objective aperture to cover the low index diffraction spots or rings of the SAED. When complete amorphization occurred, all diffraction maximum in the SAED patterns disappeared, and the amorphization fluence was recorded concurrently as the critical amorphization dose (D_c). The fluence was then converted to the universal radiation damage unit of displacements per atom (dpa) by SRIM-2008 simulations using displacement threshold energies E_d of 50 eV for Ca, P, O, and H in $\text{Ca}_{10}(\text{PO}_4)_6(\text{OH})_2$ and a

sample density of 3.16 g/cm³.

The response of HAp to electron irradiations at room temperature was investigated using a JOEL 2010 TEM at the Shared Instrumentation Facility (SIF) of Louisiana State University operated under 200 kV accelerating voltage. The microstructural evolution under electrons was monitored by both SAED and high resolution transmission electron microscopy (HRTEM) imaging. Electron irradiation fluence was calculated based on the current density of the unobstructed beam recorded on the small fluorescent screen. The current density was read directly from the small screen and reflected the electrons hitting the sample. During irradiations, the electron current density was maintained at 511.7 pA/cm². The sample was irradiated around 30 minutes and the HRTEM images were taken every 3 minutes. The images were taken quickly to reduce the irradiation caused by the focused beam when collecting and monitoring the images. Both the as-prepared HAp-600C powder and the ion-irradiated samples were used in the electron irradiation experiments. Synergistic 1 MeV Kr²⁺ and 200 keV electron irradiations were also performed using the IVEM Tandem Facility with both ion and electron beams turned on simultaneously.

3. Results and discussions

3.1 Ion-beam-irradiation induced amorphization and temperature dependence

Under 1 MeV Kr²⁺ irradiation at room temperature (298 K), HAp-600C sample underwent the crystalline-to-amorphous transformation as indicated by the SAED patterns and TEM dark field images (Fig. 2). The loss of crystallinity was evidenced by the reduced contrast in the dark field images, as well as decreased intensity of the diffraction rings and the emerging amorphous halo rings in the SAED patterns upon ion bombardment. The structure was completely amorphized at a critical dose (D_c) of 2×10^{14} ions/cm² (0.05 dpa), as the dark field contrast was lost and the diffraction rings were totally replaced by the amorphous halo rings. Irradiations at higher temperature showed remarkable temperature dependence of the amorphization process due to strong dynamic annealing of the radiation-induced defects. Although the similar radiation-induced amorphization processes still occurred at elevated temperature, the D_c for amorphization increased dramatically with the temperature. As the temperature was increased to 448K, 473K, 498K and 523K, the corresponding D_c increased to 3×10^{14} ions/cm² (0.075 dpa), 8×10^{14} ions/cm² (0.20 dpa), 8×10^{14} ions/cm² (0.20 dpa) and 1.875×10^{15} ions/cm² (0.47 dpa), respectively, in an obvious exponential manner.

The exponential increase in critical dose with the increase of temperature is a result of enhanced defect mobility and recombination rate at elevated temperature, effectively dictating the radiation-induced damage process. The crystalline to amorphous transformation under 1 MeV Kr^{2+} can be attributed to the ballistic interaction between the ions and the atoms in HAp, and the subsequent atomic displacements. This process is accompanied by simultaneous dynamic recovery of the defects, and the competition between the defect production and recovery largely determines the fate of the material. As the defect mobility and recombination rate increase at higher temperatures while the defect production remained much less affected, the radiation-induced damage is significantly suppressed, leading to higher D_c to achieve amorphization. This remarkable dynamic annealing behavior was indicated by the temperature dependence curve of D_c plotted in Fig. 3 and fitted by an empirical exponential function based on a direct impact model[21, 22] given in the equation (1), where D_0 is the critical amorphization dose extrapolated at $T = 0$ K, E_a is the defect annealing activation energy and T_c is designated as the critical amorphization temperature.

$$D_c = \frac{D_0}{1 - \exp[(E_a/K)(1/T_c - 1/T)]} \quad (1)$$

At T_c , the dynamic annealing rate of radiation defects equals defect production rate, such that amorphization can never be induced under ion irradiation. Therefore, a lower critical temperature indicates greater defect annealing and higher radiation tolerance. Irradiation data fitting found an activation energy E_a of 0.098 eV, and a T_c of 545 ± 12.8 K for the HAp-600C, which is significantly lower than most apatite structures previously reported, such as $\text{Ca}_2\text{La}_8(\text{SiO}_4)_6\text{O}_2$ silicate apatite (700 K)[23], synthetic britholite (880 K ~ 910 K) [4], Ce-doped $\text{Mg}_2\text{Y}_8(\text{SiO}_4)_6\text{O}_2$ silicate apatite (667.5 K ~ 963.6 K)[24], $\text{Ca}_{10}(\text{P}0.5\text{V}0.5\text{O}_4)_6\text{F}_2$ (562 K) and $\text{Ca}_{10}(\text{VO}_4)_6\text{F}_2$ fluorapatites (603 K)[3], suggesting excellent defect annealing capability of HAp under displacive radiations.

3.2 Electron irradiation induced recrystallization

In situ TEM study was performed to investigate the phase and microstructural changes of HAp under 200 keV electron beam irradiation. While the as-prepared nano-crystalline HAp-600C showed little changes to 200 keV electrons even at a very high dose, the ion-irradiation amorphized HAp (denoted as HAp-amph) samples exhibited an extremely high sensitivity to electron beams, as a rapid recrystallization was observed with *in situ* TEM. Fig. 4 showed the

recrystallization process of HAp-amph under current density of $J=511.7 \text{ pA/cm}^2$ of 200 keV electrons. At the beginning of the electron irradiation process shown in Fig. 4 (a), featureless amorphous zones were found in the HRTEM image, and diffraction halos without distinct extra diffraction rings or spots were seen in the SAED pattern, proving the amorphous state in the original HAp-amph. After being irradiated for 180 seconds ($6.0 \times 10^{11} \text{ e}^-/\text{cm}^2$), nano-crystals began to nucleate, marked by the arrows shown in Fig. 4 (b). As the material was continuously exposed to electrons, the recrystallization propagated as nano-crystals growth became more prominent, covering an increasing fraction of the sample (Fig. 4 (c)). The recrystallization eventually completed after 1120 seconds of electron irradiation, with a total critical fluence of $3.9 \times 10^{12} \text{ e}^-/\text{cm}^2$, at which point an average grain size of 4.3 nm with a random orientation was obtained (Fig. 4 (d)). The percent of recrystallization versus electron fluence curve manifested itself in a characteristic sigmoidal curve shape with clear nucleation and growth stages (Fig. 5). The SAED pattern obtained from the recrystallized zones showed the same structure as the original HAp-600C (Fig. 6), indicating that the recrystallization retained same phase. Although similar electron irradiation induced amorphous-to-crystalline transformations have been previously observed in Si, Ge, GaP, GaAs[25], pyrochlores[26], zircon[8], monazite[1] and silicate apatite[6, 7, 27], the amorphized HAp in the present study is extremely sensitive to electron-induced recrystallization, with a critical electron fluence of $3.9 \times 10^{12} \text{ e}^-/\text{cm}^2$ for complete recrystallization. It is the lowest in ceramic waste forms that have been reported, and indeed many orders of magnitude lower than most of the materials reported in this category, such as Si ($\sim 10^{22} \text{ e}^-/\text{cm}^2$), GaP ($\sim 10^{22} \text{ e}^-/\text{cm}^2$)[25], natural zircon ($1.69 \times 10^{23} \text{ e}^-/\text{cm}^2$)[8], LaPO_4 ($1.87 \times 10^{18} \text{ e}^-/\text{cm}^2$)[8], and CePO_4 monazite ($\sim 10^{22} \text{ e}^-/\text{cm}^2$)[1]. The stronger defect annealing ability of HAp here may be attributed to the apatite structure-type. Some studies indicated better recrystallization ability in phosphates like $\text{Ca}_5(\text{PO}_4)_3\text{F}$, berlinite AlPO_4 and monazite as a result of the lower rigidity of the PO_4 relative to SiO_4 tetrahedra in the amorphous matrix, as the PO_4 tetrahedra rotate and reorganize themselves in the recrystallization process under irradiation more easily than the other structures like SiO_4 tetrahedra which lack of double bonds.

Although the kinetics of the recrystallization shows similarity to thermally stimulated crystallization, the likelihood of electron beam heating effect as the major driving force is clearly ruled out. The maximum increase in temperature (ΔT) due to electron beam can be estimated using Fisher's model given in Equation (2)[25, 28, 29],

$$\Delta T = \frac{I}{\pi \kappa e} \left(\frac{\Delta E}{d} \right) \ln \frac{b}{r_o} \quad (2)$$

where I is beam current, κ is the thermal conductivity of the material, b is the heat sink radius in the sample, r_o is the beam radius, e is the elementary electron charge, and ΔE is the total energy loss per electron in a sample thickness of d , which can be derived from the Bethe-Bloch formula given in Equation (3)[30].

$$-\frac{dE}{dx} = \frac{2\pi Z \rho \left(\frac{e^2}{4\pi\epsilon_0} \right)^2}{mv^2} \left\{ \ln \left[\frac{E(E+mc^2)^2 \beta^2}{2I_e^2 mc^2} \right] + (1 - \beta^2) - (2 - \sqrt{1 - \beta^2} - 1 + \beta^2) \ln 2 + \frac{1}{8} (1 - \sqrt{1 - \beta^2})^2 \right\}, \quad (3)$$

where Z is the atomic number of the target, ρ is its atomic density, m is the electron mass, v is its velocity, E is electron energy, c is the speed of light, $\beta = v/c$, and I_e is the excitation energy for electrons in the target material. Based on the calculation, under 200 keV electrons, the temperature rise in HAp was estimated to be merely 0.7 K, with $I = 100$ pA, $\kappa = 0.36$ W/mk[31], $b = 1.5$ mm, $r_o = 100$ nm and $dE/dx = 0.8$ eV/nm. Therefore, electron beam induced temperature increase and hence the thermal activation of the recrystallization in HAp is negligible, which is in agreement with many other ceramic materials [8, 25, 27, 32, 33].

Notably, the electron accelerating voltage used in the irradiation (200 kV) is considered insufficient to generate significant atomic displacements. The threshold energies for displacements E_d in oxide-based ceramics are typically in the range of 20-50 eV [34]. The maximum amount of energy E_{max} that can be transferred from electrons with kinetic energy of E to a target atom is

$$E_{max} = E_0 \frac{2m}{M_A} \left[\left(\frac{E}{E_0} \right)^2 + 2 \frac{E}{E_0} \right] \quad (4)$$

where m is the mass of an electron, M_A is the mass of the target, and $E_0 = mc^2$. Accordingly, the E_{max} for the major atoms in HAp are below their threshold energy E_d , so that the atomic displacement assisted growth is unlikely. The most tenable mechanism of the sub-threshold electron irradiation induced recrystallization of HAp is the breaking and reforming of the dangling bonds along the amorphous-crystalline (a/c) interface. Compared to bonds in crystalline materials, the weak dangling bonds at the (a/c) interface are relatively easy to break under the ionizing electrons, which is followed by the rearrangement of the nearby atoms in non-equilibrium bonding configurations to form the energetically favored complete bonds, thus driving the recrystallization process. In addition, the nucleation stage is likely heterogeneous as

there could be sub-nanometer to nanometer sized residual crystals that were not completely amorphized by the preceding ion beam irradiation. These residual crystals can lower the activation energy and provide seeding sites for nucleation to proceed at an enhanced rate. The recrystallization curve is in good agreement with the Avrami-Erofeev model[35],

$$f = 1 - \exp[-(kt)^n], \quad (5)$$

where f is the crystallization fraction, k is temperature dependent rate constant, and n is JMAK exponent. The parameters n and k were determined by fitting the data using the Avrami-Erofeev Equation (5) to be 2.56 and 2.72, respectively, implying a two dimensional growth.

3.3 Synergistic effect of ion and electron beam irradiation

Concurrent ion and electron irradiations were also performed to investigate the stability of nanocrystalline HAp-600C under the influence of both alpha and beta decay events. Fig. 7 showed the set of SAED patterns of HAp-600C irradiated simultaneously by simultaneous 1 MeV Kr^{2+} ions and 200 keV electron beam at room temperature. It is noted that, at an irradiation dose of 0.05 dpa, which is the D_c measured in the single ion beam irradiation at room temperature, the SAED pattern still largely retained the diffraction rings with significant contrast in the dark field image, clearly indicating the crystalline state of the sample. The crystalline structure remained until the dose reached 0.15 dpa, 3 times of the D_c under single ion beam irradiation, demonstrating a significant delay of the displacive ion-induced amorphization process at the presence of the sub-threshold ionizing electrons, which strongly boost the recovery of the radiation-induced defect, a trend that is consistent with the recrystallization behavior of pre-amorphized HAp under 200 keV electrons. In a nuclear waste repository environment that contains both α -emitters (*e.g.* actinides) and β -emitters (*e.g.* fission products), the long-term stability of HAp-based waste form could be greatly enhanced, owing to the extremely high sensitivity of the material to ionization-assisted defect recovery induced by β -decay events.

4. Conclusions

A systematic experimental investigation of the radiation stability of hydroxyapatite has been reported in the present work. The nano-crystalline hydroxyapatite or HAp samples were prepared by a simple and efficient method of calcining bovine bones at 600°C for 60 minutes. Displacive ion irradiation using 1 MeV Kr^{2+} reveals a crystalline-to-amorphous transformation in HAp, similar to many ceramic-based waste form materials. However, HAp also exhibits strong dynamic defect annealing reflected by a dramatically increased critical amorphization dose at

higher temperature, with a critical temperature of 545 ± 12.8 K and an activation energy of 0.098 eV. More remarkably is its extremely high sensitivity to ionizing electron irradiation induced defect recovery process, especially its rapid recrystallization behavior under the sub-threshold 200 keV electrons. The electron fluence needed to complete the recrystallization at room temperature is merely $3.9 \times 10^{12} \text{ e}^-/\text{cm}^2$, many orders of magnitude lower than most ceramics and the lowest among candidates for ceramic nuclear waste forms. The rapid recrystallization is attributed to interface dangling bond breaking and rearranging under electron bombardments, without the assistance of thermally stimulated processes. Synergistic 1 MeV Kr^{2+} and 200 keV electron irradiations further prove the high defect recovery in HAp assisted by the ionizing electrons, as the D_c in this case is enhanced to three times of that under ion irradiation alone, indicating a significantly improved radiation stability, a characteristic that is especially important to the design of highly durable materials to be deployed in intensive radiation conditions.

Acknowledgements

The work was supported by Louisiana State University Office of Research & Economic Development (ORED) Faculty Research Grant, and Louisiana Board of Regents LINK program under the contract number NSF(2015)-LINK-97. The authors thank the staff of the IVEM-Tandem facilities at Argonne National Laboratory, Marquis Kirk and Peter Baldo, for their assistance in ion irradiations and *in situ* TEM observation.

The data that support the findings of this study are available from the corresponding author, [F.Y. Lu and J.R. Zhou], upon reasonable request.

References

- [1] F. Lu, Y. Shen, X. Sun, Z. Dong, R.C. Ewing, J. Lian, Size dependence of radiation-induced amorphization and recrystallization of synthetic nanostructured CePO_4 monazite, *Acta Materialia* 61(8) (2013) 2984-2992.
- [2] J. Zhang, J. Lian, A.F. Fuentes, F. Zhang, M. Lang, F. Lu, R.C. Ewing, Enhanced radiation resistance of nanocrystalline pyrochlore $\text{Gd}_2(\text{Ti}_{0.65}\text{Zr}_{0.35})_2\text{O}_7$, *Applied Physics Letters* 94(24) (2009) 243110.
- [3] F. Lu, Z. Dong, J. Zhang, T. White, R.C. Ewing, J. Lian, Tailoring the radiation tolerance of vanadate-phosphate fluorapatites by chemical composition control, *RSC Advances* 3(35) (2013) 15178-15184.
- [4] S. Utsunomiya, S. Yudinsev, L. Wang, R. Ewing, Ion-beam and electron-beam irradiation of synthetic britholite, *Journal of Nuclear Materials* 322(2) (2003) 180-188.
- [5] F. Lu, J. Zhang, M. Huang, F. Namavar, R.C. Ewing, J. Lian, Phase transformation of nanosized ZrO_2 upon thermal annealing and intense radiation, *The Journal of Physical Chemistry C* 115(15) (2011) 7193-7201.
- [6] I.-T. Bae, Y. Zhang, W.J. Weber, M. Ishimaru, Y. Hirotsu, M. Higuchi, Temperature dependence of electron-beam induced effects in amorphous apatite, *Nuclear Instruments and Methods in Physics Research Section B: Beam*

Interactions with Materials and Atoms 266(12) (2008) 3037-3042.

- [7] I.-T. Bae, Y. Zhang, W.J. Weber, M. Ishimaru, Y. Hirotsu, M. Higuchi, Ionization-induced effects in amorphous apatite at elevated temperatures, *Journal of Materials Research* 23(04) (2008) 962-967.
- [8] A. Meldrum, L. Boatner, R. Ewing, Electron-irradiation-induced nucleation and growth in amorphous LaPO₄, ScPO₄, and zircon, *Journal of materials research* 12(7) (1997) 1816-1827.
- [9] W. Suchanek, M. Yoshimura, Processing and properties of hydroxyapatite-based biomaterials for use as hard tissue replacement implants, *Journal of Materials Research* 13(01) (1998) 94-117.
- [10] R. Suganthi, S.P. Parthiban, K. Elayaraja, E. Girija, P. Kulariya, Y. Katharria, F. Singh, K. Asokan, D. Kanjilal, S.N. Kalkura, Investigations on the in vitro bioactivity of swift heavy oxygen ion irradiated hydroxyapatite, *Journal of Materials Science: Materials in Medicine* 20(1) (2009) 271-275.
- [11] T. Wen, X. Wu, M. Liu, Z. Xing, X. Wang, A.-W. Xu, Efficient capture of strontium from aqueous solutions using graphene oxide–hydroxyapatite nanocomposites, *Dalton Transactions* 43(20) (2014) 7464-7472.
- [12] S.H. Tan, X.G. Chen, Y. Ye, J. Sun, L.Q. Dai, Q. Ding, Hydrothermal removal of Sr²⁺ in aqueous solution via formation of Sr-substituted hydroxyapatite, *Journal of hazardous materials* 179(1-3) (2010) 559-563.
- [13] M.J. Rigali, P.V. Brady, R.C. Moore, Radionuclide removal by apatite, *American Mineralogist* 101(12) (2016) 2611-2619.
- [14] R.J. Turner, J.C. Renshaw, A. Hamilton, Biogenic Hydroxyapatite: A New Material for the Preservation and Restoration of the Built Environment, *ACS applied materials & interfaces* 9(37) (2017) 31401-31410.
- [15] A. Coulon, A. Grandjean, D. Laurencin, P. Jollivet, S. Rossignol, L. Campayo, Durability testing of an iodate-substituted hydroxyapatite designed for the conditioning of ¹²⁹I, *Journal of Nuclear Materials* 484 (2017) 324-331.
- [16] A. Coulon, D. Laurencin, A. Grandjean, C.C.D. Coumes, S. Rossignol, L. Campayo, Immobilization of iodine into a hydroxyapatite structure prepared by cementation, *Journal of Materials Chemistry A* 2(48) (2014) 20923-20932.
- [17] L. Wang, J. Chen, R. Ewing, Radiation and thermal effects on porous and layer structured materials as getters of radionuclides, *Current Opinion in Solid State and Materials Science* 8(6) (2004) 405-418.
- [18] S. Dey, J.W. Drazin, Y. Wang, J.A. Valdez, T.G. Holesinger, B.P. Uberuaga, R.H. Castro, Radiation Tolerance of Nanocrystalline Ceramics: Insights from Yttria Stabilized Zirconia, *Scientific reports* 5 (2015).
- [19] D. Chen, F. Gao, B. Liu, Grain boundary resistance to amorphization of nanocrystalline silicon carbide, *Scientific reports* 5 (2015).
- [20] I. Beyerlein, A. Caro, M. Demkowicz, N. Mara, A. Misra, B. Uberuaga, Radiation damage tolerant nanomaterials, *Materials today* 16(11) (2013) 443-449.
- [21] S. Wang, L. Wang, R. Ewing, Irradiation-induced amorphization: Effects of temperature, ion mass, cascade size, and dose rate, *Physical Review B* 63(2) (2000) 024105.
- [22] W. Weber, Models and mechanisms of irradiation-induced amorphization in ceramics, *Nuclear Instruments and Methods in Physics Research Section B: Beam Interactions with Materials and Atoms* 166 (2000) 98-106.
- [23] J. Lian, L. Wang, K. Sun, R.C. Ewing, In situ TEM of radiation effects in complex ceramics, *Microscopy research and technique* 72(3) (2009) 165-181.
- [24] J. Zhou, T. Yao, J. Lian, Y. Shen, Z. Dong, F. Lu, Radiation-induced amorphization of Ce-doped Mg₂Y₈(SiO₄)₆O₂ silicate apatite, *Nuclear Instruments and Methods in Physics Research Section B: Beam Interactions with Materials and Atoms* 379 (2016) 102-106.
- [25] I. Jencic, M. Bench, I. Robertson, M. Kirk, Electron-beam-induced crystallization of isolated amorphous regions in Si, Ge, GaP, and GaAs, *Journal of Applied Physics* 78(2) (1995) 974-982.
- [26] Z. Huang, J. Qi, L. Zhou, Z. Feng, X. Yu, Y. Gong, M. Yang, Q. Shi, N. Wei, T. Lu, Fast crystallization of amorphous Gd₂Zr₂O₇ induced by thermally activated electron-beam irradiation, *Journal of applied physics* 118(21) (2015) 214901.
- [27] I.-T. Bae, Y. Zhang, W.J. Weber, M. Higuchi, L.A. Giannuzzi, Electron-beam induced recrystallization in amorphous apatite, *Applied physics letters* 90(2) (2007) 21912-21912.

- [28] A. Meldrum, L. Boatner, R. Ewing, Electron-irradiation-induced nucleation and growth in amorphous LaPO_4 , ScPO_4 , and zircon, *Journal of materials research* 12(07) (1997) 1816-1827.
- [29] S. Fisher, On the temperature rise in electron irradiated foils, *Radiation effects* 5(2) (1970) 239-243.
- [30] H. Bethe, J. Ashkin, *Experimental Nuclear Physics*, ed. E. Segré, J. Wiley, New York, (1953) 253.
- [31] T. Coelho, E. Nogueira, W. Weinand, W. Lima, A. Steimacher, A. Medina, M. Baesso, A. Bento, Thermal properties of natural nanostructured hydroxyapatite extracted from fish bone waste, *Journal of applied physics* 101(8) (2007) 084701.
- [32] Y. Zhang, J. Lian, C.M. Wang, W. Jiang, R.C. Ewing, W.J. Weber, Ion-induced damage accumulation and electron-beam-enhanced recrystallization in SrTiO_3 , *Physical Review B* 72(9) (2005) 094112.
- [33] J. Frantz, J. Tarus, K. Nordlund, J. Keinonen, Mechanism of electron-irradiation-induced recrystallization in Si, *Physical Review B* 64(12) (2001) 125313.
- [34] S. Zinkle, C. Kinoshita, Defect production in ceramics, *Journal of Nuclear Materials* 251 (1997) 200-217.
- [35] R.M. Roque-Malherbe, *The physical chemistry of materials: Energy and environmental applications*, CRC Press 2009.

Caption of figures

Fig. 1 XRD pattern (Red line) and the Rietveld refinement result (blue line) of the nano-crystalline hydroxyapatite sample, showing the $\text{Ca}_{10}(\text{PO}_4)_6(\text{OH})_2$ apatite structure of the sample calcined at 600°C

Fig. 2 Room temperature TEM bright field image, dark field images and selected area diffraction patterns of (a) Bright field image (b) the unirradiated and (c) 1 MeV Kr^{2+} irradiated at 0.05 dpa, indicating the ion irradiation induced amorphization process

Fig. 3 Temperature dependence of the critical dose of the nano-crystalline hydroxyapatite sample calcined at 600°C

Fig. 4 Room temperature structural changes of Kr^{2+} induced amorphous nano-crystalline hydroxyapatite under the 200 keV irradiation: (a) 0 s, (b) 180 s ($6.0 \times 10^{11} \text{ e}^-/\text{cm}^2$), (c) 640 s ($2.13 \times 10^{12} \text{ e}^-/\text{cm}^2$), (d) 1120 s ($3.73 \times 10^{12} \text{ e}^-/\text{cm}^2$), (e) digitally processed image from the area marked in (d)

Fig. 5 Recrystallization percent of amorphous nano-crystalline hydroxyapatite sample as a function of different current electron fluence, varying from 0 to $4.53 \times 10^{12} \text{ e}^-/\text{cm}^2$

Fig. 6 Diffraction patterns under different electron fluence: a) Diffraction pattern of pre-amorphized sample; b) Diffraction pattern at 1440s ($3.9 \times 10^{12} \text{ e}^-/\text{cm}^2$) under electron beam irradiation at room temperature; c) Diffraction pattern of unirradiated sample at room temperature

Fig. 7 Room temperature TEM dark field image and selected area diffraction patterns of (a) the unirradiated HAP-600C, (b) concurrent ion and electron irradiated HAP-600C at 0.05 dpa, and (c) concurrent ion and electron irradiated HAP-600C at 0.15 dpa. The amorphization trend is significantly delayed owing to the electron beam assisted defect recovery

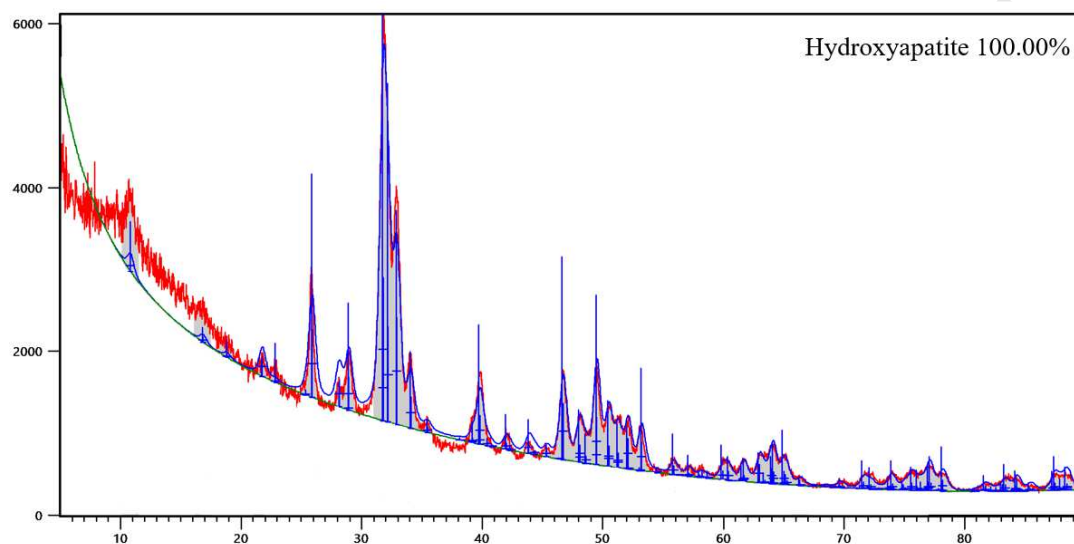


Fig. 1 XRD pattern (Red line) and the Rietveld refinement result (blue line) of the nano-crystalline hydroxyapatite sample, showing the $\text{Ca}_{10}(\text{PO}_4)_6(\text{OH})_2$ apatite structure of the sample calcined at 600°C

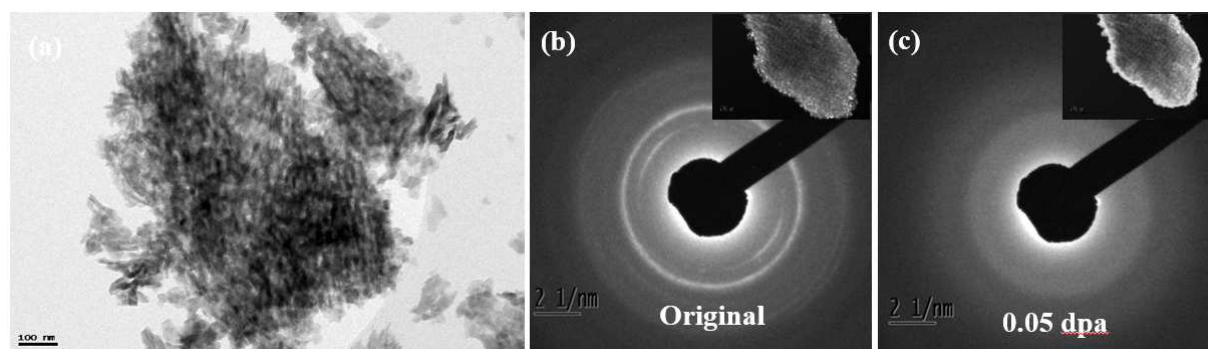


Fig. 2 Room temperature TEM bright field image, dark field images and selected area diffraction patterns of (a) Bright field image (b) the unirradiated and (c) 1 MeV Kr^{2+} irradiated at 0.05 dpa, indicating the ion irradiation induced amorphization process

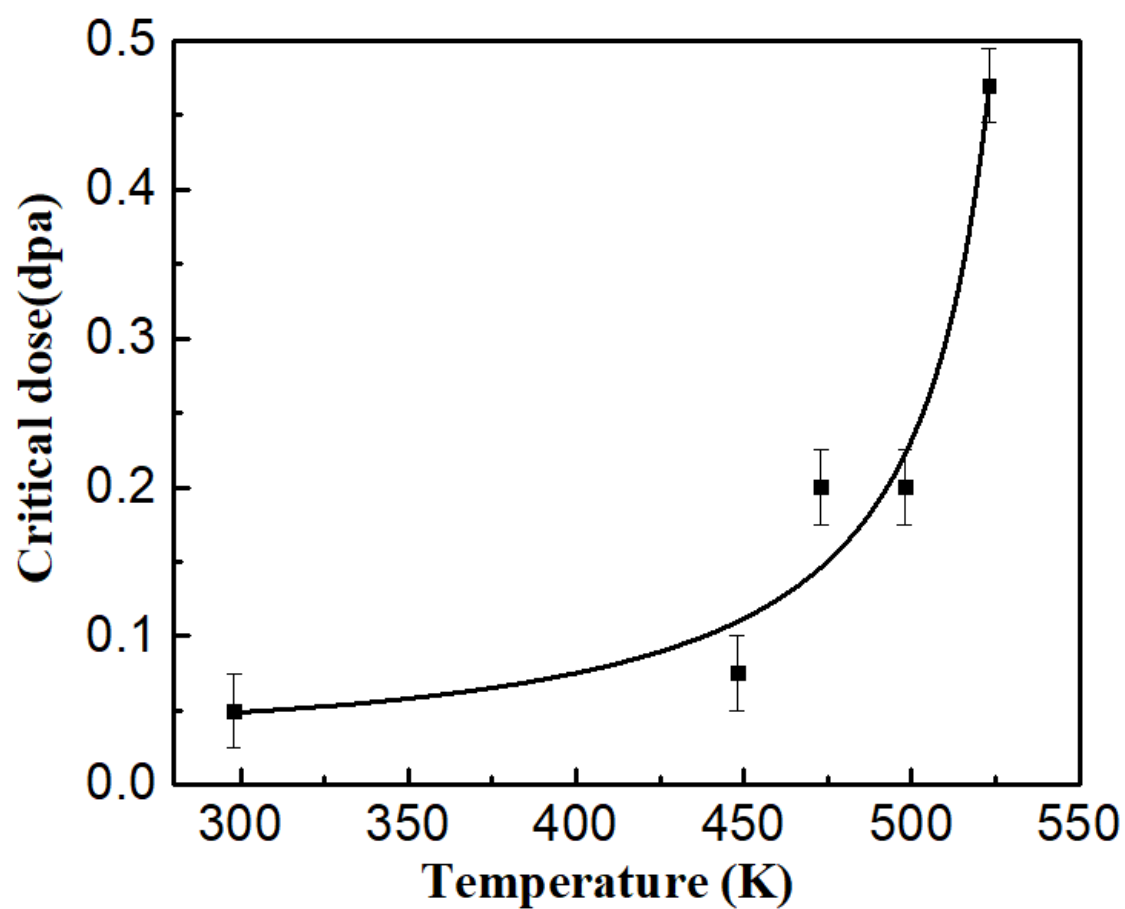


Fig. 3 Temperature dependence of the critical dose of the nano-crystalline hydroxyapatite sample calcined at 600°C

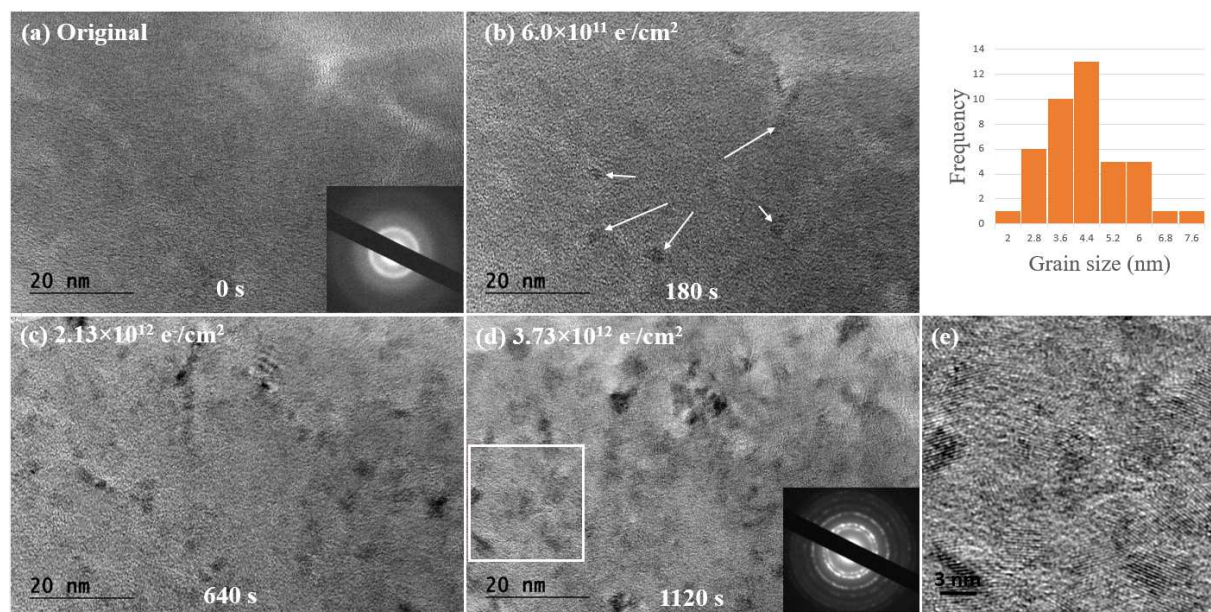


Fig. 4 Room temperature structural changes of Kr^{2+} induced amorphous nano-crystalline hydroxyapatite under the 200 keV irradiation: (a) 0 s, (b) 180 s ($6.0 \times 10^{11} \text{ e}^-/\text{cm}^2$), (c) 640 s ($2.13 \times 10^{12} \text{ e}^-/\text{cm}^2$), (d) 1120 s ($3.73 \times 10^{12} \text{ e}^-/\text{cm}^2$), (e) digitally processed image from the area marked in (d)

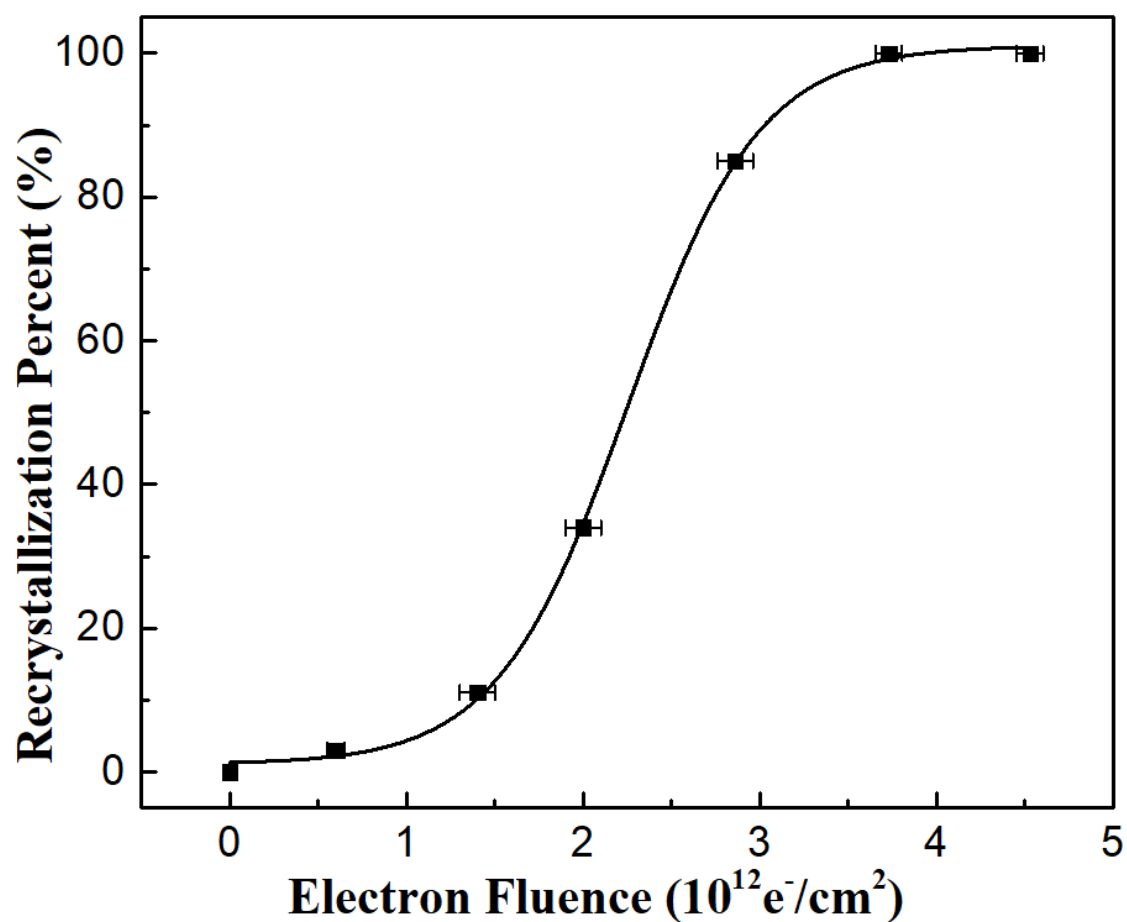


Fig. 5 Recrystallization percent of amorphous nano-crystalline hydroxyapatite sample as a function of different current electron fluence, varying from 0 to $4.53 \times 10^{12} \text{ e}^-/\text{cm}^2$

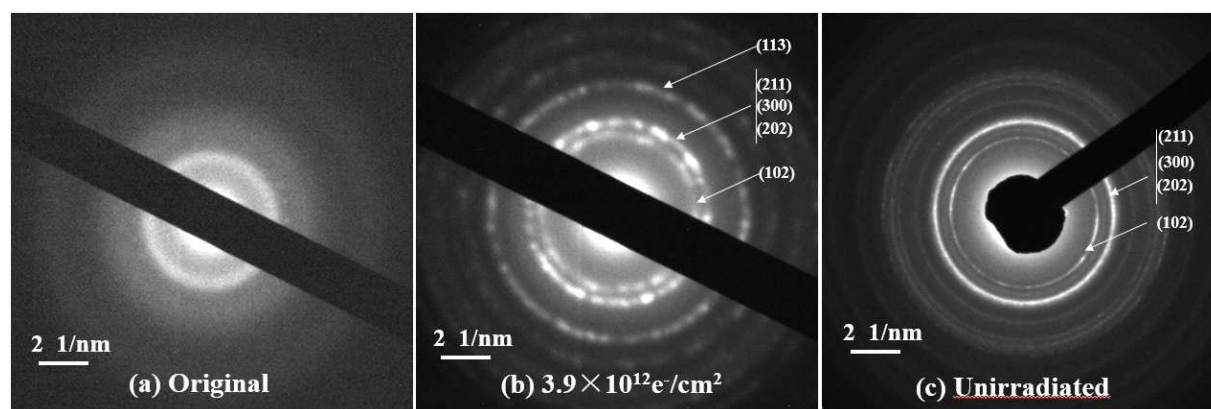


Fig. 6 Diffraction patterns under different electron fluence: a) Diffraction pattern of pre-amorphized sample; b) Diffraction pattern at 1440s ($3.9 \times 10^{12} \text{ e}^-/\text{cm}^2$) under electron beam irradiation at room temperature; c) Diffraction pattern of unirradiated sample at room temperature

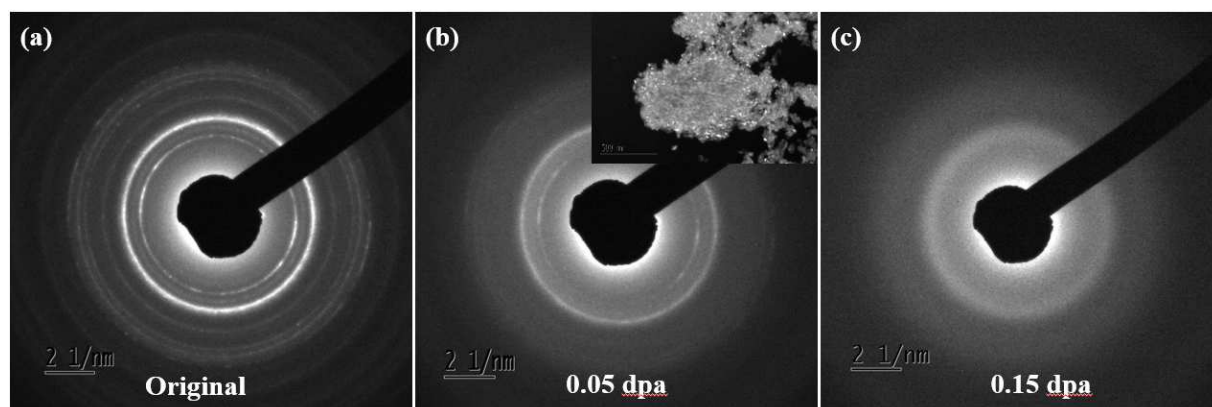


Fig. 7 Room temperature TEM dark field image and selected area diffraction patterns of (a) the unirradiated HAP-600C, (b) concurrent ion and electron irradiated HAP-600C at 0.05 dpa, and (c) concurrent ion and electron irradiated HAP-600C at 0.15 dpa. The amorphization trend is significantly delayed owing to the electron beam assisted defect recovery